Supporting Information

Defect-mediated hierarchical tubular $CoSe_2$@TiO_2 heterostructure photocatalysts for boosted CO_2 photoreduction

Jing Lin, Yajie Chen, Li Kan, Xinyan Yu, Guohui Tian*

Key Laboratory of Functional Inorganic Material Chemistry, Ministry of Education of the People's Republic of China, Heilongjiang University, Harbin 150080 P. R. China

*Corresponding author; E-mail: tiangh@hlju.edu.cn

1. Experimental section

1.1 Characterization of photocatalysts

The crystal phase, morphology and structure of the samples were determined by X-ray diffraction analysis (XRD, SmartLab 9 KW, Rigaku), scanning electron microscope (SEM, Sigma 500, ZEISS), transmission electron microscope (TEM, JEM F200, JEOL) and Raman spectra (HR 800, Jobin Yvon). The chemical state of the samples was investigated in detail using X-ray photoelectron spectroscopy (XPS, Axis Ultra DLD, Kratos). UV-visible absorption spectra were obtained using an ultraviolet-visible spectrophotometer (Lambda 950, PerkinElmer). The oxygen vacancies were determined using an electron paramagnetic resonance spectrometer (EPR, EMXplus, Bruker). Photoluminescence (PL) spectra were recorded with a fluorescence spectrophotometer (FLS 920P, Edinburgh). N_2 adsorption-desorption isotherms and CO_2 adsorption tests were performed on ASAP 2420 from Micromeritics. CO_2 temperature programmed desorption (CO_2-TPD) experiments were conducted using a chemisorption analyzer (ChemBET Pulsar). In situ diffuse reflectance infrared Fourier transform spectroscopy (DRIFTS) was obtained from a Fourier Transform Infrared Spectrometer (in situ FTIR, Nicolet iS50, Thermo Scientific).

1.2 Photoelectrochemical measurements

The electrochemical impedance spectroscopy (EIS), Mott-Schottky curves and transient photocurrent curves (IT) of the prepared samples were tested using the CHI 660E electrochemical workstation with a standard three-electrode system. During the measurements, a platinum sheet and a saturated calomel electrode were selected as the counter electrode and reference electrode, respectively. The working electrode with the sample coated on the conductive side was immersed in a 0.5 M sodium sulfate electrolyte solution and driven under a 300 W Xe lamp equipped with an AM 1.5 G filter.

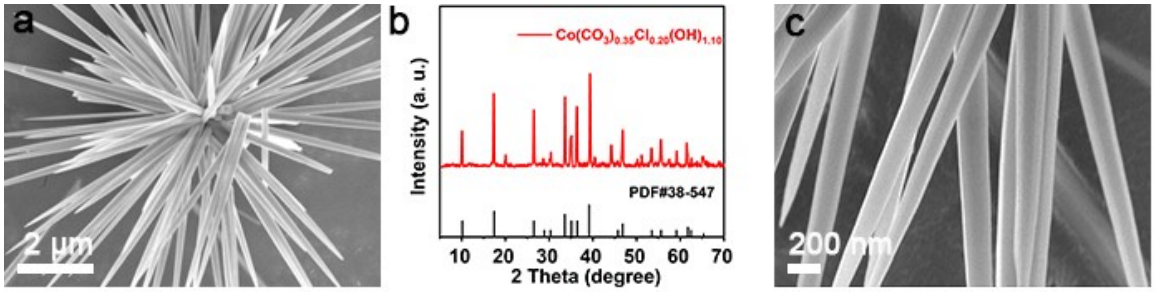

Fig. S1. (a, c) SEM images and (b) XRD pattern of $Co(CO_3)_{0.35}Cl_{0.20}(OH)_{1.10}$.

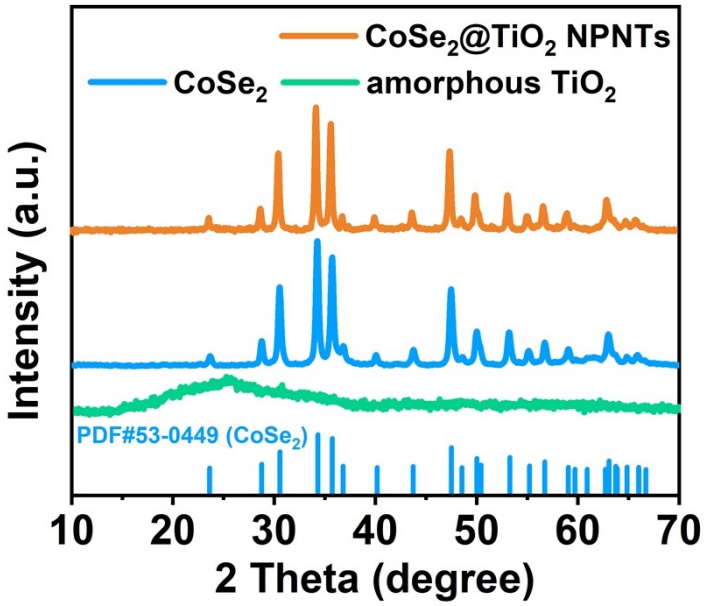

Fig. S2. XRD patterns of the different samples.

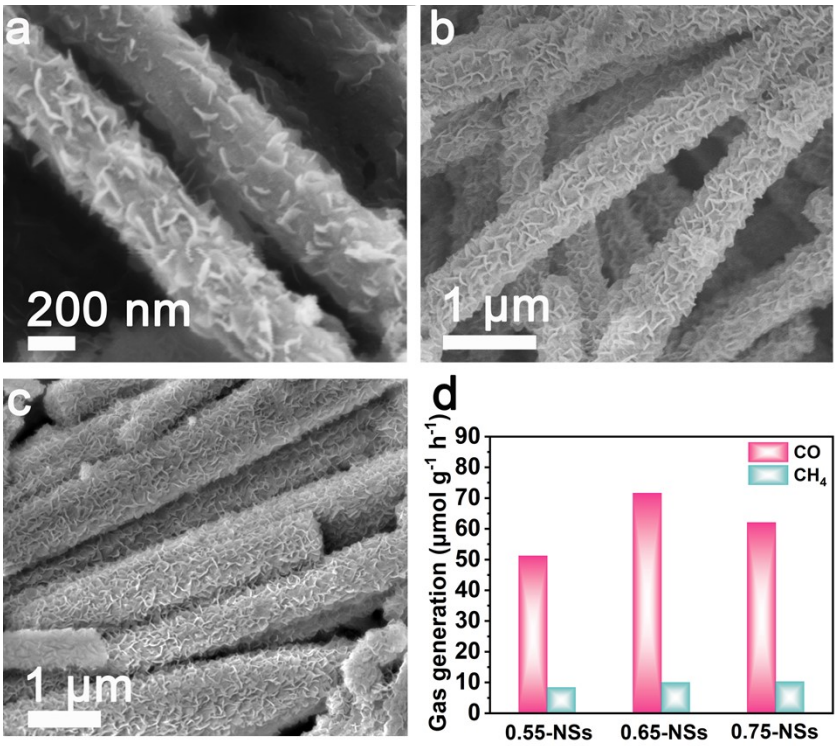

Fig. S3. SEM images of $CoSe_2$@TiO_2 NSNTs with different TiO_2 contents: (a) $CoSe_2$@TiO_2-0.55, (b) $CoSe_2$@TiO_2-0.65, (c) $CoSe_2$@TiO_2-0.75 and (d) corresponding average evolution yields of CO and CH_4 with different TiO_2 loading.

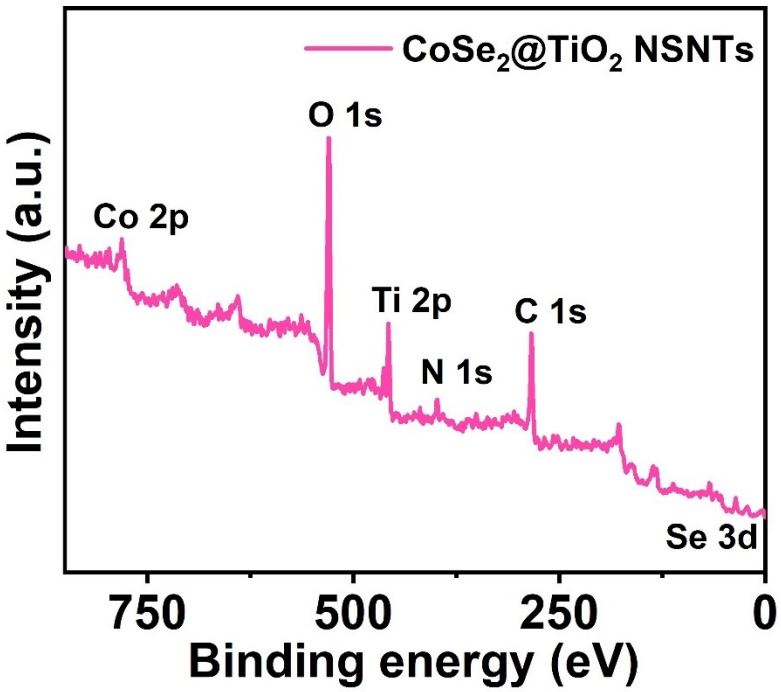

Fig. S4. XPS full-spectrum of $CoSe_2$@TiO_2 NSNTs.

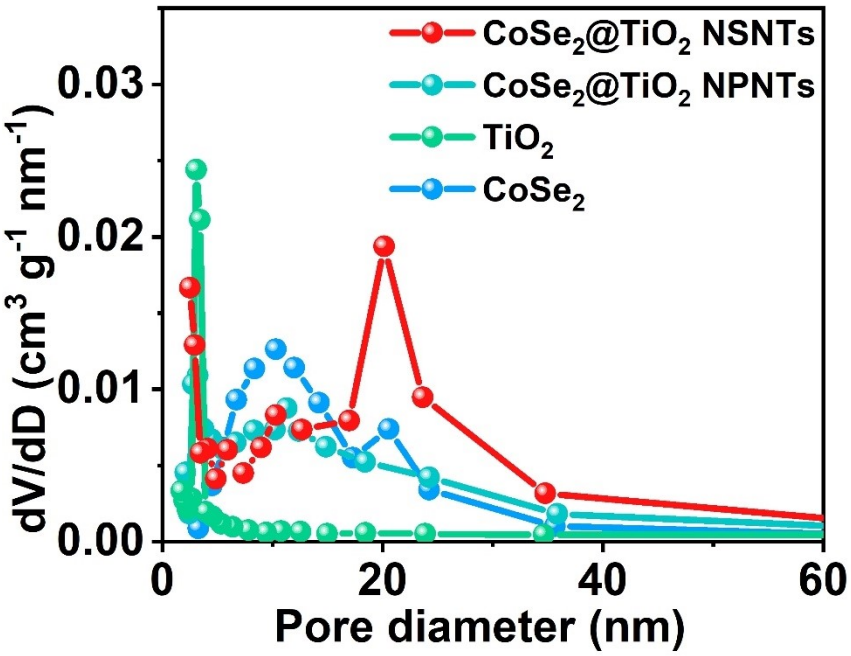

Fig. S5. The corresponding pore size distributions of the different samples.

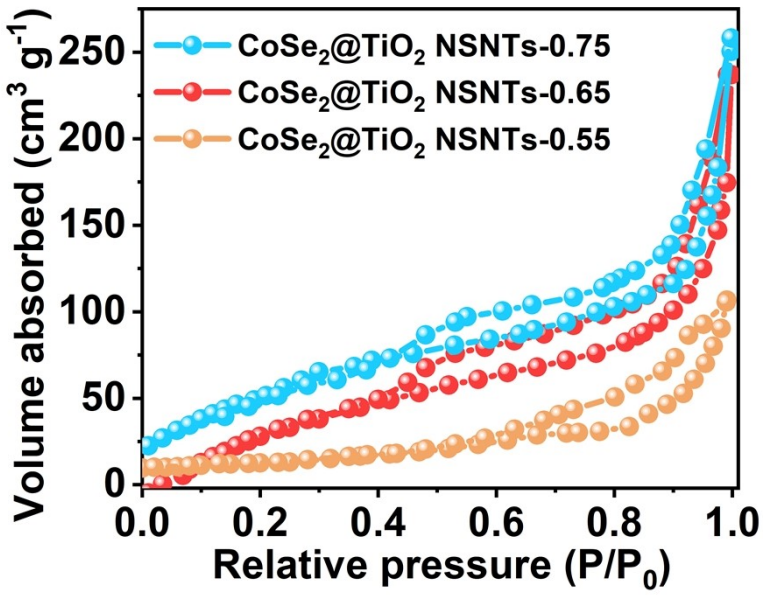

Fig. S6. N_2 adsorption-desorption isotherms of $CoSe_2$@TiO_2 NSNTs with different TiO_2 contents.

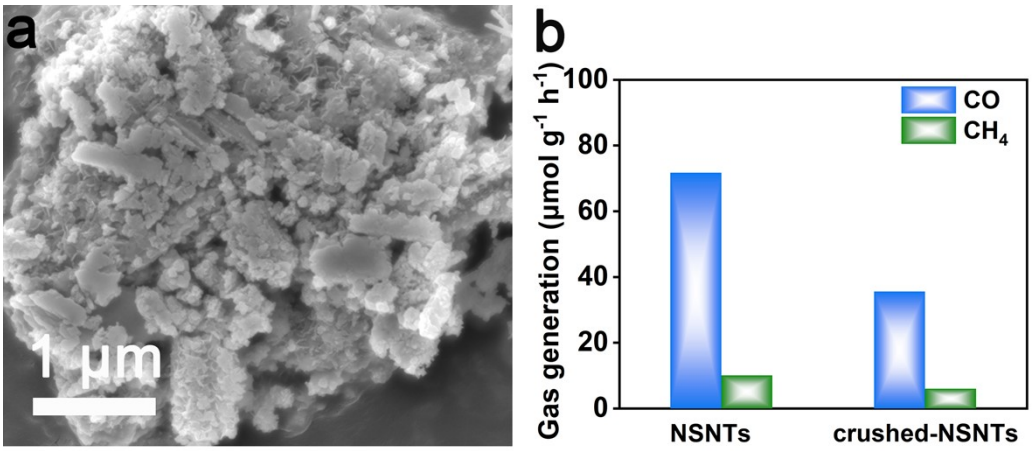

Fig. S7. (a) SEM image of the crushed $CoSe_2$@TiO_2 NSNTs and (b) CO_2 photoreduction performance of $CoSe_2$@TiO_2 NSNTs and the crushed-$CoSe_2$@TiO_2 NSNTs.

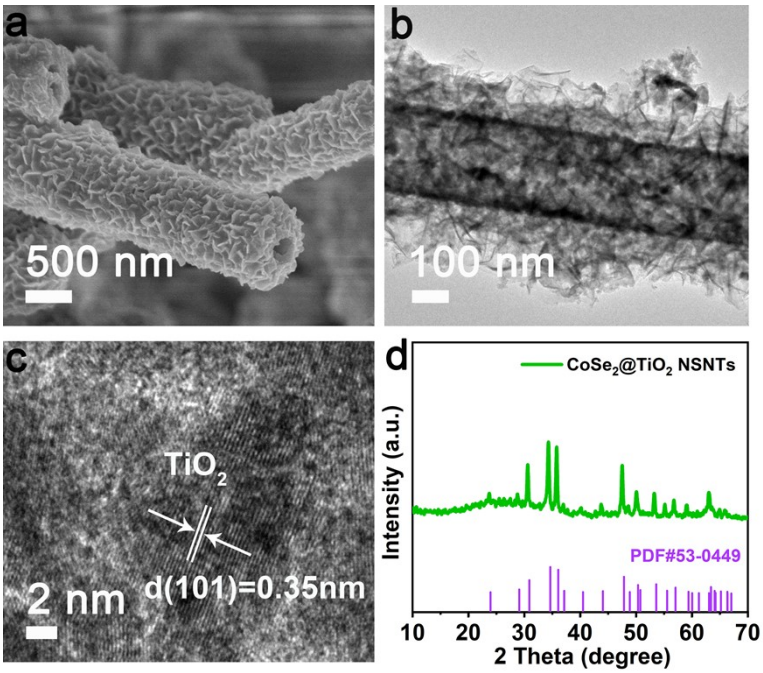

Fig. S8. Morphology and structure characterizations of $CoSe_2$@TiO_2 NSNTs after four cycles. (a) SEM, (b) TEM, and (c) HRTEM images; (d) XRD pattern.

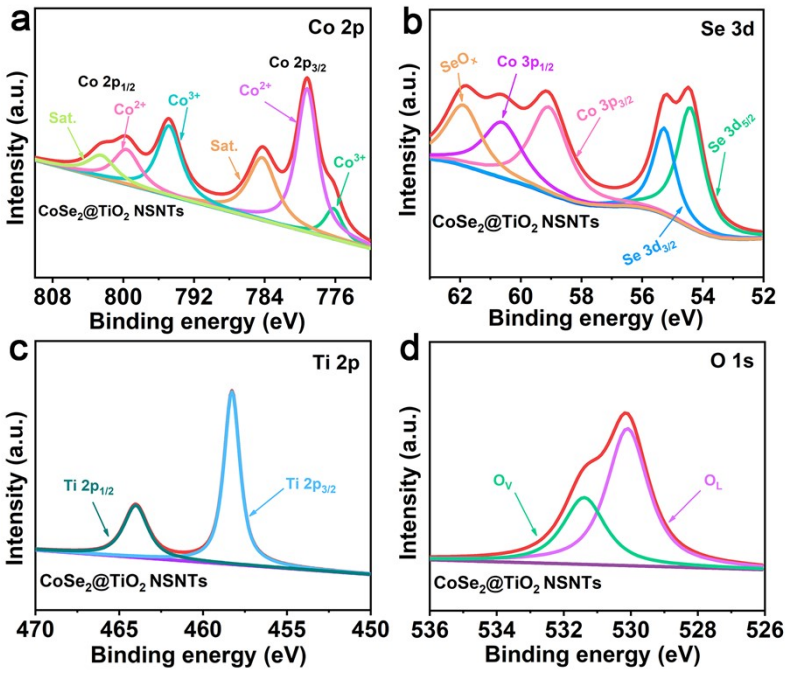

Fig. S9. High-resolution XPS spectra of (a) Co 2p, (b) Se 3d, (c) Ti 2p and (d) O 1s of $CoSe_2$@TiO_2 NSNTs after 16 hours.

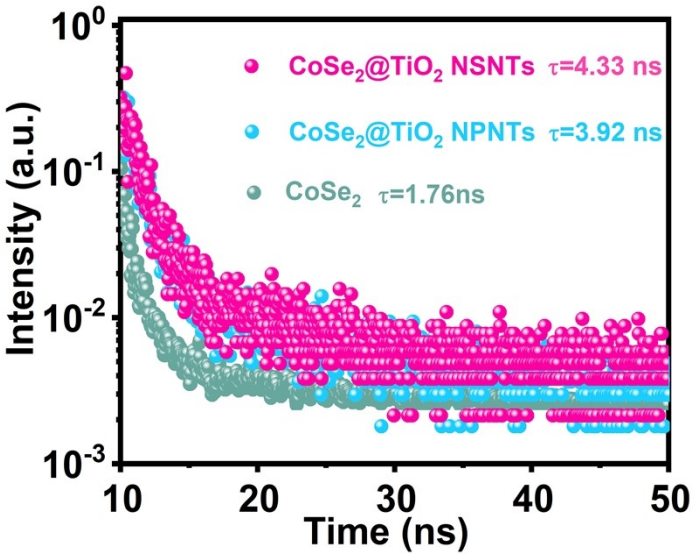

Fig. S10. TRPL spectra.

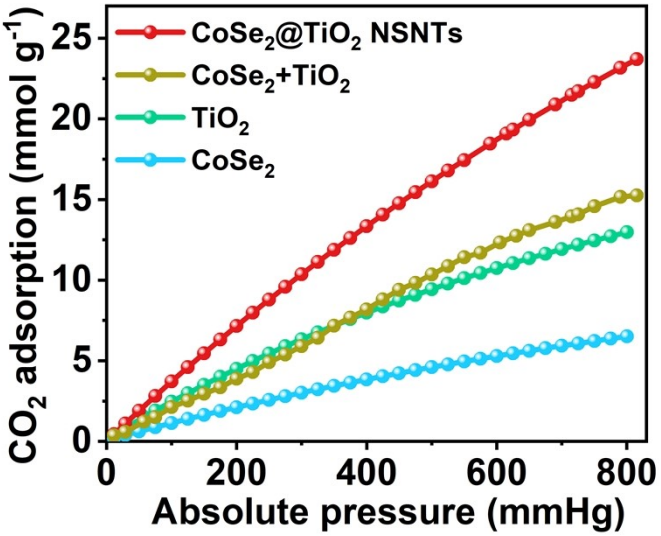

Fig. S11. CO_2 adsorption isotherms of $CoSe_2$@TiO_2 NSNTs and the control samples.

Table S1. BET surface area, pore volume, average pore size for $CoSe_2$, TiO_2, $CoSe_2$@TiO_2 NPNTs, and $CoSe_2$@TiO_2 NSNTs.

Samples	S_{BET} (m^2 g^{-1})	Pore volume (cm^3 g^{-1})	Average pore size (nm)
$CoSe_2$	80.1	0.136	19.8
TiO_2	93.2	0.171	5.5
$CoSe_2$@TiO_2 NPNTs	65.8	0.156	17.6
$CoSe_2$@TiO_2 NSNTs	105.5	0.162	21.8

Table S2. The determined energy band parameters of the samples

Photocatalyst	E_g (eV)	E_f (V)	XPS (VB) (eV)	E_{VB} (V)	E_{CB} (V)
$CoSe_2$	1.55	-0.53	1.46	0.93	-0.62
TiO_2	3.11	-0.46	3.01	2.55	-0.56

Table S3. The results of photoreduction of the as-prepared samples.

Samples	Yield of CO ($\mu mol\ g^{-1}\ h^{-1}$)	Yield of CH_4 ($\mu mol\ g^{-1}\ h^{-1}$)	CO selectivity (%)
$CoSe_2$	17.53	5.73	43.3
TiO_2	33.09	5.31	60.9
$CoSe_2$@ TiO_2 NPNTs	50.64	6.34	66.6
$CoSe_2$@ TiO_2 NSNTs	71.71	10.09	63.9

Table S4. The results of photoreduction of the as-prepared samples.

Samples	Yield of CO ($\mu mol\ g^{-1}\ h^{-1}$)	Yield of CH_4 ($\mu mol\ g^{-1}\ h^{-1}$)
$CoSe_2$	17.53	5.73
TiO_2	33.09	5.31
$CoSe_2$@ TiO_2 NPNTs	50.64	6.34
$CoSe_2$@ TiO_2 NSNTs-0.55	51.27	8.43
$CoSe_2$@ TiO_2 NSNTs-0.65	71.71	10.09
$CoSe_2$@ TiO_2 NSNTs-0.75	62.11	10.33

Table S5. Comparison of the activity of $CoSe_2$@TiO_2 NSNTs with recently reported catalysts for the photocatalytic reduction of CO_2 to CO and CH_4.

Photocatalyst	Light source	CO Yield ($\mu molg^{-1} h^{-1}$)	CH_4 Yield ($\mu mol\ g^{-1} h^{-1}$)	Ref.
TiO_2@$ZnIn_2S_4$ CSHS	300 W Xenon lamp	9.28	4.26	[S1]
In/TiO_2-V_O	320 nm<λ<780 nm 0.20 W cm^{-2} Xenon lamp	3.37	35.49	[S2]
TiO_2/$CsPbBr_3$	300 W Xenon lamp	9.02	/	[S3]
$Co_{0.85}$Se-CdSe/$MoSe_2$ /CdSe	300 W Xenon lamp	15.04	0.41	[S4]
WO_3-TiO_2/Cu_2ZnSnS_4	400 W Xenon lamp	15.37	1.69	[S5]
$CoSe_2$@TiO_2 NSNTs	300 W Xenon lamp	71.71	10.09	This work

References

[S1] L. Wang, B. Cheng, L. Zhang and J. Yu, *Small*, 2021, **17**, 2103447.

[S2] C. Chen, L. Chen, Y. Hu, K. Yan, T. Wang, Y. Huang, C. Gao, J. Mao, S. Liu and B. Li, *J. Energy Chem.*, 2023, **86**, 599-608.

[S3] F. Xu, K. Meng, B. Cheng, S. Wang, J. Xu and J. Yu, *Nat Commun*, 2020, **11**, 4613.

[S4] L. Du, Y. Chen, Q. Wang, Y. Zhao, L. Li, X. Liu and G. Tian, *Small*, 2021, **17**, 2100412.

[S5] A. Raza, H. Shen, A. A. Haidry, L. Sun, R. Liu and S. Cui, *J. CO_2 Util.*, 2020, **37**, 260-271.